Singlet Fission within Diketopyrrolopyrrole Nanoparticles in Water

Catherine M. Mauck, Patrick E. Hartnett, Yi-Lin Wu, Claire E. Miller, Tobin J. Marks,* and Michael R. Wasielewski*

Department of Chemistry, Argonne-Northwestern Solar Energy Research (ANSER) Center, and Institute for Sustainability and Energy at Northwestern, Northwestern University, Evanston, Illinois 60208-3113, United States

* Supporting Information

ABSTRACT: Nanoparticles (NPs) of the singlet fission chromophore 3,6-bis(5-phenylthiophen-2-yl)pyrrolo[3,4-c]pyrrole-1,4(2H,5H)-dione (PhTDPP) having average hydrodynamic diameters of 63−193 nm were prepared by rapidly injecting variable concentrations of PhTDPP solutions in tetrahydrofuran into water. These PhTDPP NPs are stable over months in water and exhibit fluorescence quantum yields ≪1%. Femtosecond transient absorption spectros-copy shows that singlet fission is more rapid in smaller NPs, likely reflecting their greater surface area-to-volume ratio and consequent exposure of more molecules to the high dielectric aqueous environment. These observations suggest that charge transfer states, whose energy is sensitive to the dielectric constant of the surrounding medium, serve as virtual intermediates in PhTDPP NP singlet fission. However, the lifetime of the triplet excitons produced by singlet fission is longest in the larger NPs having greater long-range order, which allows the triplet excitons to diffuse further from one another thus slowing triplet−triplet annihilation.

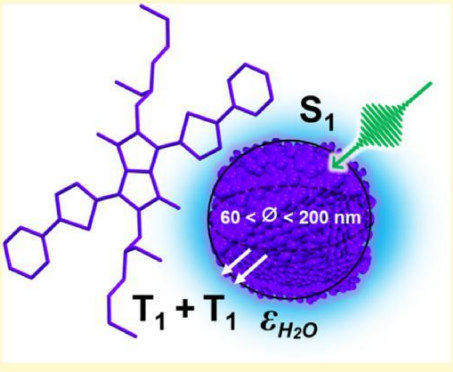

INTRODUCTION

Singlet fission (SF) is the spontaneous spin-allowed formation of two triplet excitons from one singlet exciton following absorption of a single photon in an array of two or more organic chromophores. SF can achieve up to a 200% triplet exciton quantum efficiency in single crystals, thin films, and molecular dimers in solution.[1] As a result, SF molecules have received ever-increasing attention for applications in organic photovoltaics (OPVs), as well as hybrid and dye-sensitized solar cells as a result of their potential for carrier multiplication.[2−6] A variety of chromophores have been studied to answer fundamental questions about the SF mechanism, including pentacene,[7−10] tetracene,[11−16] carotenoids,[17−19] diphenyliso-benzofuran,[20,21] rylene derivatives,[8,22,23] and a handful of other molecular systems.[24−27] In an effort to interpret experimental results and predict molecular structures that can undergo high yield SF, theoretical studies have proposed several different mechanisms, often focusing on the role of charge transfer (CT) states as real or virtual intermediates that facilitate SF.[10,28,28−32]

Recently, we observed SF for the first time in diketopyrro-lopyrroles (DPPs),[29] a class of chromophores widely used in OPVs. DPPs are known for their strong visible absorption, high electron mobilities, and photochemical stability.[30−34] In thin films of 3,6-di(5-phenylthiophen-2-yl)pyrrolo[3,4-c]pyrrole-1,4(2H,5H)-dione (PhTDPP), the SF rate constant is $k_{SF} = 4.6 \times 10^9$ s^{-1} with a triplet yield of 165 ± 30%.[29] A further study on 3,6-di(thiophen-2-yl)pyrrolo[3,4-c]pyrrole-1,4-(2H,5H)-dione (TDPP) with different N-alkyl chain sub-stituents demonstrated that crystal morphology has a strong effect on SF yield as well as mechanism, with the observation of an excimer-like dark state that promotes SF, which is assigned to the correlated triplet pair ^{1}(TT) state having overall singlet character.[29]

The degree of CT character between adjacent TDPP molecules was hypothesized to influence the SF rate since different solid state packing geometries were seen to modulate donor−acceptor interactions between molecules. Electronic asymmetry in the immediate vicinity of any given pair of chromophores will dictate whether the relevant states are CT states or charge resonance (CR) states that are characteristic of excimers formed from two equivalent chromophores.[35−38] Recent calculations on the influence of virtual CT state energies in DPP and other chromophores indicate that such states should affect DPP SF rates via a superexchange mechanism.[39] Thus, the role of CT or CR states on DPP SF requires further experimental elucidation.

Colloidal NPs of tetracene and pentacene derivatives in aqueous media have previously been prepared and charac-terized using optical spectroscopy.[40−43] Carotenoids have also been studied in aggregate assemblies.[17,18] Additionally, the polar aqueous environment surrounding the NPs may provide the electronic asymmetry needed to create virtual CT states having an energy low enough to promote SF via the superexchange mechanism.[25] In a study of diphenyltetracene (DPT) NPs, precipitation yielded 11 nm diameter NPs with an estimated 50% of the chromophores in contact with the

aqueous environment. Despite the high surface-to-volume ratio and a SF rate similar to that in thin films, the triplet yield was half that of the DPT film, and the authors concluded that CT states are not directly populated intermediates in DPT SF.[40] This same approach can be adapted to investigate SF in PhTDPP NPs dispersed in aqueous solutions. In this study we prepare very robust PhTDPP NPs and show that they undergo SF to form triplet excitons in hundreds of picoseconds and remain stable in aqueous solution for months. We find that the SF rate depends on NP size, as NPs with higher surface area-to-volume ratios exhibit faster SF rates. We also observe that the decay of the triplet excitons is slower in NPs with larger crystalline domains, which mitigates against triplet−triplet annihilation. Although this process limits high triplet yields in PhTDPP NPs, this study demonstrates that DPP NPs are promising materials for studying SF in solution. Thus, the strategic design of intermolecular interactions in DPP NPs may yield longer-lived triplet excitons, of interest for useful singlet oxygen generation in aqueous solution.[44,45]

EXPERIMENTAL METHODS

Nanoparticle Preparation. PhTDPP was synthesized as described previously.[29] Its chemical structure along with its absorption spectrum are shown in Figure 1. NP preparation is performed by the reprecipitation method[40,46] in which a solution of PhTDPP in THF (200 μL) at a specified concentration (50, 100, 250, and 500 mM) is injected rapidly into deionized water (10 mL) while rapidly stirring. Upon injection, NP nucleation leads to bright blue solutions, with negligible variation in the absorption spectrum as a function of NP size.

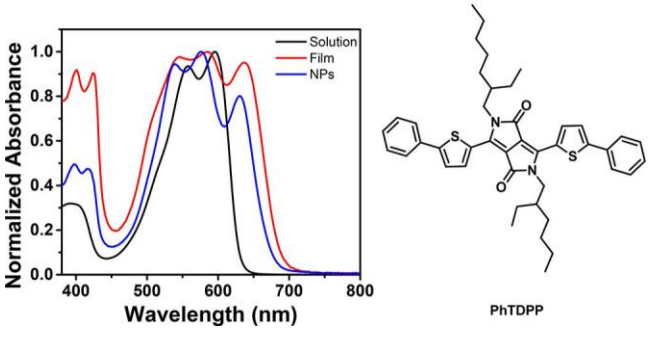

Figure 1. Normalized steady-state optical absorption spectra for PhTDPP (right): solution monomer (black), annealed film (red), and 63 nm diameter NPs in water (blue).

Steady-State Characterization. UV−vis absorption spectra were acquired on a Shimadzu UV-1800 spectrophotometer. Particle size and size distribution were measured on a Malvern NanoSight LM10-HS or NS300 instrument, using NP tracking analysis (NTA). The NTA-based microscopic method visualizes the light scattered by the NPs when illuminated by a laser source. Brownian motion of each NP is tracked in real-time simultaneously but separately by the image analysis program to determine the distribution in hydrodynamic diameters based on the rate of NP movement, temperature, and viscosity of the liquid.

Small Angle X-ray Scattering (SAXS) Measurements. SAXS data were acquired at beamline 12ID-B at the Advanced Photon Source (APS), Argonne National Laboratory using a Pilatus 2 M detector with 14 keV incident radiation. Samples were loaded into 2 mm quartz capillaries with a wall thickness of 0.2 mm, and 30−60 sequential data frames with exposure times of 1 s were recorded, reduced, and averaged for each measurement. Sample solutions were oscillated using a syringe pump during data collection to prevent radiation damage. Scattering intensity is reported as a function of the modulus of the scattering vector q, related to the scattering angle 2θ by $q = (4\pi/\lambda) \sin\theta$, where λ is the X-ray wavelength (14 keV, 0.918 Å) in the range of $q \sim 0.005-0.5$ Å^{-1}. Subtracting the solvent scattering intensity ($I_{solvent}$) from the sample scattering (I_{sample}) gives the scattering contributed by the NPs ($I_{NP} = I_{sample} - I_{solvent}$).

Femtosecond Transient Absorption Spectroscopy (fsTA). Experimental details for fsTA experiments have been described elsewhere.[29] Briefly, the output of a 100 kHz amplifier at 1040 nm (4.5 W, 350 fs, Spirit 1040-4, Spectra Physics) passes through a beam splitter to direct 510 mW to generate a white light continuum probe pulse (490−1100 nm) in a 5 mm undoped yttrium aluminum garnet (YAG) crystal and 2.66 W to drive a noncollinear optical parametric amplifier (Spirit-NOPA 3H, Spectra Physics) which generates 75 fs pump pulses. Pump and probe polarizations are set to the magic angle relative to one another and are spatially and temporally overlapped at the sample. The pump spot size was set to 1.08 mm with per-pulse energies of 10−20 nJ (1.1−2.2 μJ/cm^2). Once passed through the sample, the probe beam is dispersed using a custom designed concave grating spectrometer that utilizes a 430 groove/mm concave holographic reflectance grating with an image focal distance of 85.4 mm. The dispersed probe pulses are detected using a commercial 100 kHz CMOS line scan camera (AViiVA EM4 from E2 V). The pump beam is chopped at 50 kHz prior to the sample. NP suspensions were prepared fresh prior to fsTA experiments and were excited at 525 nm in a 2 mm path length cuvette. To achieve high enough optical densities for fsTA measurements, the as-synthesized NPs were concentrated using Amicon Ultra-4 centrifugal filters with Ultracel-10 membranes (Millipore), with no change in the steady-state absorption spectra or the measured hydrodynamic diameter for centrifuged vs as-synthesized NPs (Figure S1).

RESULTS AND DISCUSSION

Nanoparticle Size. Particle size can be controlled by varying the concentration of the injection solution, i.e., from 50 to 500 mM, achieving mean hydrodynamic diameters of 63, 75, 90, and 193 nm. We will refer to each NP sample by their average particle diameter. Average NP diameters and the number of PhTDPP molecules per NP, n, for each injection concentration are summarized in Table 1, as measured by Nanoparticle Tracking Analysis (NTA).[47] Estimations of n assume spherical NPs having the same density as the PhTDPP crystal structure (1 molecule/0.866 nm^3). As surface disorder and decreased density due to solvent penetration are both likely in NPs,[40] this represents an upper bound. The steady-state absorption spectra for PhTDPP NPs of different sizes are shown in Figure 2.

Table 1. Measured Hydrodynamic Diameters for PhTDPP NPs as a Function of Injection, Full Width at Half Maximum (fwhm), Calculated Number of PhTDPP Molecules per NP, n, and Surface Area-to-Volume Ratio SA:V

concn	peak (nm)	fwhm (nm)	n (× 10^5)	SA:V
50 mM	63	46	1.5	0.012
100 mM	75	52	2.6	0.010
250 mM	90	70	4.6	0.008
500 mM	193	207	36	0.004

Steady-State Optical Characterization. NP absorption spectra are compared to that of monomeric PhTDPP in solution and to a vapor-deposited PhTDPP film in Figure 1. PhTDPP has two peaks at 595 and 557 nm in solution because the DPP absorption shifts to redder wavelengths with increasing conjugation.[48] This characteristic visible transition has been assigned to π−π* intramolecular charge transfer (ICT) to the lactam core in similar DPP molecules.[49]

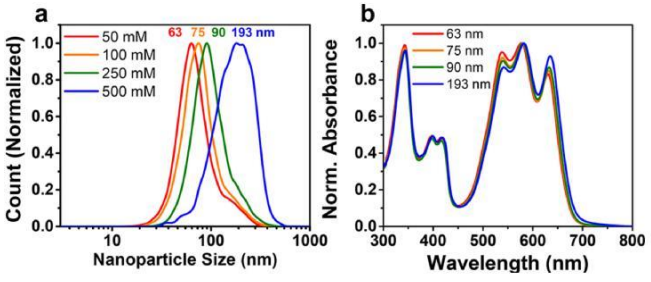

Figure 2. (a) NP size distribution as a function of initial injection concentration. (b) Absorption spectra of PhTDPP NPs with 63−193 nm diameters.

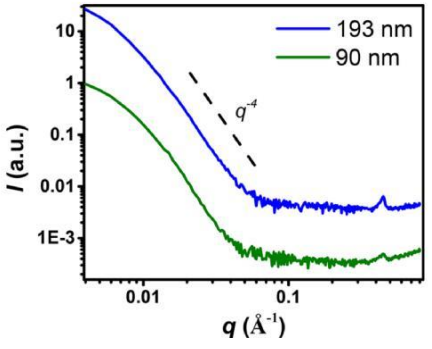

Figure 3. SAXS/WAXS data for 193 nm diameter (blue) and 90 nm diameter (green) NPs in solution.

Intermolecular interactions in the solid thin film[29,33,49,50] lead to broadening of the absorption accompanied by the enhancement of a lower energy band, with peaks at 636, 588, and 545 nm. NP absorption spectra are similar to the film spectra, with peaks at 630, 575, and 539 nm. However, the overall absorption is narrower than in the film, with sharper peaks. In addition, the π−π* band at ~400 nm is more intense in the film than in the NPs. As the NP size increases, only small changes in the absorption spectra are evident, with the absorption peak at 636 nm increasing in intensity relative to the declining feature at 557 nm. This trend indicates a negligible increase in intermolecular coupling since the overall absorption spectra change very little with NP size.[29,49,50] A small redshift of the overall absorption also occurs (~5 nm from 63 to 193 nm NPs).

Monomeric PhTDPP is highly fluorescent in solution with a fluorescence quantum yield Φ_F = 0.59 in CH_2Cl_2.[29] In contrast to the solution phase, PhTDPP NPs have $\Phi_F \leq 0.3\%$ (Table S1), indicating that the singlet excited state is substantially quenched by a kinetically competitive, intermolecular process. This is consistent with the behavior of PhTDPP thin films which have $\Phi_F \leq 0.3\%$ due to SF.[29] The steady-state fluorescence spectra for 193 nm diameter NPs are broadened and red-shifted, lacking the strong vibronic progression of monomeric PhTDPP fluorescence (Figure S2).

Nanoparticle Stability and Structural Characteriza-tion. Although previous studies of tetracene and pentacene-based NPs have shown that their spectra change fairly rapidly following preparation,[40,41,43] the steady-state absorption spectra of the PhTDPP NP solutions change very little over months after their preparation. Similarly, centrifugal concentration of the NPs prior to fsTA measurements has little effect on either the steady-state absorption spectra or the transient absorption spectra and kinetics (Figure S1).

Small-angle X-ray scattering measurements (SAXS) were conducted to study chromophore order within the NPs.[44] The scattering intensity (I) vs the modulus of the scattering vector (q) shown in Figure 3 displays a slope of −4 in the Porod region, suggesting that the NPs are spherical, and this result supports the shape assumption used in calculating the average number of molecules per NP and the surface area-to-volume ratio. More importantly, distinct NP diffraction is observed at q ~ 0.4 Å^{-1} for the 90 and 193 nm diameter NP solutions, while the diffraction is too weak to be measured for the smaller NPs. The SAXS peak at q ~ 0.4 Å^{-1} can be attributed to the diffraction from the (001) facets based on the X-ray single-crystal structure of PhTDPP.[29] By performing Scherrer analysis,[51] we find that the correlation lengths along the [001] crystal axis are 13 and 8 nm for 193 and 90 nm NPs, respectively. If we assume the same molecular density as in the crystal structure, these domains correspond to 34 and 22 PhTDPP molecules for the 193 and 90 nm NPs, respectively. On the previously characterized thin films of PhTDPP,[29] we estimate 20 nm domains by applying the same analysis, which corresponds to 51 DPPs. Thus, we find that the NPs have domain sizes smaller than in the thin film, with domain size decreasing with NP diameter, as expected. Note that greater disorder in the NPs is likely, in comparison to a polycrystalline film, and therefore the calculated domain size may overestimate the number of DPPs per domain.

Femtosecond Transient Absorption Spectroscopy (fsTA). Representative selected fsTA traces for 63 nm NPs are shown in Figure 4a. The overall spectra are similar for all NP sizes. Following excitation at 525 nm with energies of 20 nJ/pulse (2.2 μJ/cm^2), sharp negative peaks appear at 533, 587, and 640 nm, representing the ground state bleach (GSB). A broad photoinduced excited state absorption (ESA) spans 676−800 nm, which slightly increases in intensity for several ps then decays as the GSB decreases. By 1 ns the triplet spectrum of PhTDPP remains, with negative peaks at 542, 591, and 644 nm and positive peaks at 564 and 616 nm. The 1 ns spectra for all NP sizes, which overlap heavily with the GSB, match the triplet spectrum of PhTDPP, as determined in thin films from SF and triplet sensitization.[29] The similarity of the NP triplet spectrum to the thin film triplet spectrum is shown in Figure S3.

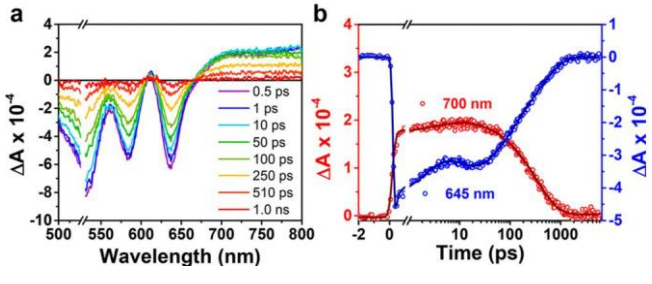

Figure 4. Selected fsTA spectra for 63 nm NPs (a) and (b) single wavelength kinetic traces at 646 nm (blue) and 700 nm (red) with associated fits τ_{rise} = 4.2 ± 0.6 ps and τ_{decay} = 330 ± 5 ps at 646 nm and τ_{decay1} = 2.4 ± 0.3 ps, τ_{rise} = 10 ± 2 ps, τ_{decay2} = 77 ± 9 ps, and τ_{decay3} = 420 ± 20 ps at 700 nm.

To characterize the kinetic behavior following photo-excitation of the PhTDPP NPs, the single wavelength kinetic traces at 700 nm (S_1 ESA) and 645 nm (GSB and $T_1 \rightarrow T_n$) were analyzed. The resulting traces and fits for 63 nm NPs are

shown in Figure 4b. At 700 nm, a rise component of 4.2 ± 0.6 ps is followed by a 330 ± 5 ps decay. In contrast, more complicated kinetics are evident at 645 nm. Following a 2.4 ± 0.3 ps fall in amplitude, a growth in GSB intensity occurs in 10 ± 2 ps. An increase in the GSB suggests that more molecules in excited states are being created than are accountable by photoexcitation alone. SF is one pathway by which a chromophore can interact with a photoexcited neighbor, such that its ground state is depopulated. In this scenario, the intensity at 645 nm can be fit to a biexponential decay of 77 ± 9 ps (40%) and 420 ± 20 ps (60%). Although the PhTDPP triplet spectrum is evident by 1 ns, it decays more rapidly than does the triplet spectrum of the film, where the SF triplet persists beyond the 8 ns time scale of the experiment.

To extract the spectral components corresponding to the multiple rise and decay components seen in the single wavelength traces, a global analysis was performed on the two-dimensional data sets by fitting selected multiple wavelengths to a specified kinetic model in a custom MATLAB program.[52] The specified rate matrix assumes unity quantum yield for each step because without adequate reference compounds to provide intrinsic competing decay processes, incorporation of loss pathway fit parameters would lead to an underdetermined matrix. Therefore, the output represents effective rate constants.

A variety of kinetic models were considered, such as a simpler three state model and parallel competing pathways of excimer formation vs SF. However, to capture the full dynamics of the NPs and in particular the 2−4 ps rise time component in Figure 4b, four sequential components were required, in order to achieve successful fit convergence and spectra that reflected the relevant states known from our previous DPP studies.[29,53]

We note that the time constants obtained by global analysis assume homogeneous populations of molecules that experience the same environment. This assumption is useful for making comparisons between the NPs as a function of size but is not completely justified; for example, surface molecules vs molecules at the NP core will experience dramatically different dielectric constants, and surface disorder or solvent penetration may induce further heterogeneity.[29,41,43]

Nonetheless, we find this model fits the kinetic data well and is useful to extract information about how the system evolves differently across the NP sizes. Thus, the best fit was achieved with the kinetic model of eq 1

$$\frac{d[S_1^*]}{dt} = -1/\tau_1[(S_1^*S_0)]$$

$$\frac{d[S_1]}{dt} = 1/\tau_1[(S_1^*S_0)] - 1/\tau_2[(S_1S_0)]$$

$$\frac{d[^1(TT)]}{dt} = 1/\tau_2[(S_1S_0)] - 1/\tau_3[^1(TT)]$$

$$\frac{d[T]}{dt} = 1/\tau_3[^1(TT)] - 1/\tau_4[T]_1 \quad (1)$$

in which the initially hot excited state ($S_1^*S_0$) relaxes (τ_1) to (S_1S_0), as the NPs are excited above the 0−0 band; from this state, the correlated triplet pair ^{1}(TT) is formed in τ_2; and finally the triplet pair undergoes fission to form triplet (T_1) in τ_3 followed by decay to the ground state with lifetime τ_4. The resulting species-associated spectra (SAS) are very similar for each NP size. Representative spectra, kinetics, and model populations for 193 nm NPs are given in Figure 5. The associated kinetic lifetimes are shown in Table 2 and plotted vs NP diameter in Figure S4 for all NP sizes. Kinetic fits and model populations for the 63, 75, and 90 nm NPs are shown in Figure S5.

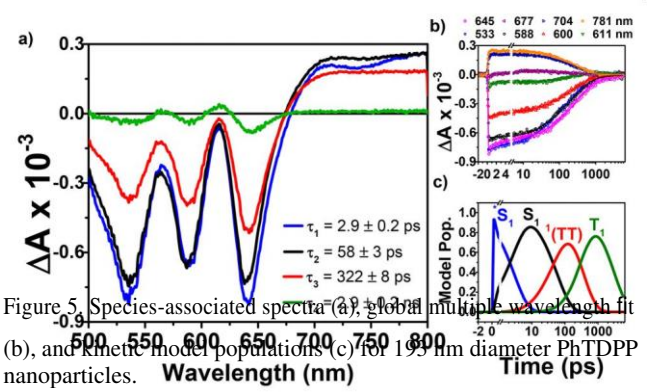

Figure 5. Species-associated spectra (a), global multiple wavelength fit (b), and kinetic model populations (c) for 193 nm diameter PhTDPP nanoparticles.

Table 2. Time Components from Global Kinetic Analysis for the Decay of ($S_1^*S_0$) (τ_1), (S_1S_0) (τ_2), ^{1}(TT) (τ_3), and T_1 (τ_4) for Different NP Samples

NP size	τ_1 (ps)	τ_2 (ps)	τ_3 (ps)	τ_4 (ps)
63 nm	1.2 ± 0.2	16 ± 1	200 ± 5	843 ± 60
75 nm	2.4 ± 0.2	25 ± 2	190 ± 7	775 ± 40
90 nm	1.6 ± 0.2	38 ± 2	310 ± 9	1370 ± 180
193 nm	2.9 ± 0.2	59 ± 3	323 ± 8	2960 ± 300

As expected for a relaxation process, τ_1 is essentially independent of NP size and shows no power dependence at the pulse energies studied (0.9−9 μJ/cm^2) (Figure S6). The redshift of the initial stimulated emission feature at 735 to 745 nm and short time scale of τ_1 suggest that it may derive from some vibrational relaxation,[54−56] but DPPs can also undergo geometric relaxation via planarization of the thiophene rings, enhancing the intramolecular CT character in the S_1 state.[49,57,54−56] The stimulated emission at 745 nm is weaker than that at 735 nm and disappears entirely as the nonemissive correlated triplet pair ^{1}(TT) is formed (τ_3). The 650−800 nm spectral region of Figure 5 is expanded and normalized to the GSB in Figure S7 to highlight the changes in the stimulated emission features of S^*S_0 and S_1S_0. The ^{1}(TT) state in the NPs has a flat, broad ESA similar to ^{1}(TT) in TDPP thin films.[29] In addition, the bleach intensity decreases at 535 nm relative to the other bleach peaks, as the triplet feature overlaps with the ground state absorption.

The final species-associated spectrum corresponds to the $T_1 \leftarrow T_n$ transition measured in a film of PhTDPP (Figure S3). We term this final state T_1, but the triplets generated are likely still in close proximity to one another given the quick decay of this state, presumably through annihilation. Further information on how quickly the triplet pair decoheres or dissociates must be studied using spin resonance techniques, as has been recently applied to several acene systems, which requires triplets which live into the ns regime.[58−60]

We find that τ_2, i.e. the formation of ^{1}(TT), slows as the NPs become larger. We have observed excimerlike intermediates

previously in TDPP thin films with strong CR interactions.[29] In NPs with smaller diameters, the CT character of the ^{1}(TT) state can be enhanced by the larger surface area-to-volume ratios, where the DPP molecules at the surface of these NPs should experience the asymmetric high dielectric aqueous environment to a greater extent.

We focus next on the triplet formation time τ_3, which is identified as τ_{SF}, the SF time constant. Compared to previous studies on PhTDPP SF in thin films (τ_{SF} = 220 ± 20 ps), triplet exciton formation in the NPs occurs slightly faster in the 63 nm (τ_{SF} = 190 ± 7 ps) and 75 nm (τ_{SF} = 200 ± 8 ps) diameter NPs, respectively, and slower in the 90 nm (τ_{SF} = 310 ± 9 ps) and 193 nm (τ_{SF} = 323 ± 8 ps) diameter NPs, respectively. If CT states are involved in PhTDPP SF, an increase in the dielectric constant should affect the SF rate as follows: if the CT state is directly populated prior to triplet formation, SF should slow as the CT state falls in energy and becomes a trap. If the higher-lying virtual CT state participates in a super-exchange SF mechanism, the SF rate should increase.[40] In this case, to understand the divergent trend in the observed PhTDPP NP SF rates, it is necessary to consider that the effects of coupling vs energetics are not easily separated. Indeed, in addition to intermolecular coupling,[11, 14,16,22,29,47] the interplay between crystallinity,[61] NP diameter, and dielectric environ-ment will determine how favorable the SF process is.

Although the larger NPs have the greatest long-range order here compared to the small NPs, domain sizes in all NPs appear to be significantly smaller than in the film, and therefore the effect of crystallinity appears to be overshadowed by exposure to the aqueous environment as expressed by the surface-to-volume ratio, as dictated by the NP diameter. Assuming spherical NPs with diameters corresponding to the peak in their size distributions, the NP sizes are 1.0, 1.8, 3.0, and 30 × 10^6 nm^3 for 63, 75, 90, and 193 nm diameter NPs (Table 1). Therefore, the surface area-to-volume ratios for the 63 and 75 nm NPs are ~0.01 nm^{-1} and 0.012 nm^{-1}, respectively. In contrast, the 90 and 193 nm NPs have lower ratios of ~0.008 nm^{-1} and 0.004 nm^{-1}, respectively. This result argues that NPs with a larger proportion of PhTDPP molecules at the surface exhibit faster SF rates, while SF is slower in the larger NPs, where a smaller proportion of molecules experience the high dielectric environment which lowers the energy of the virtual CT state and promotes SF in DPP.

Triplet Exciton Decay. As NP size and crystalline domain length increase, the triplet exciton lifetime τ_4 gets longer. Because SF relies on triplet diffusion to separate the triplets before they undergo triplet−triplet annihilation or recombine via fusion,[1,62−64] it follows that larger crystalline domains facilitate longer-lived triplets, with the largest exciton diffusion lengths observed in single crystals.[63] Both geminate and nongeminate triplet−triplet interactions are possible,[62,65,66] and the triplet exciton lifetimes observed here for even the largest NPs are quite short. Since the domain sizes in the NPs are much smaller than in PhTDPP thin films, triplet−triplet annihilation in the NPs appears to play a significant role. Bimolecular fluorescence was previously observed in DPT NPs, demonstrating that triplet−triplet annihilation can be significant in SF NPs.[40]

Polycrystalline thin films typically have shorter triplet lifetimes than single crystals.[67−69] However, triplet−triplet annihilation was recently found to be faster in more crystalline domains, with a preferential diffusion of triplet excitons to amorphous domains in TIPS-pentacene films.[64] In the present work the fastest triplet exciton decay is in the smallest NPs which likely have smaller domains according to the SAXS results. The shorter triplet lifetimes of smaller NPs can then be understood if it is assumed that a majority of the NPs are polycrystalline but with decreasing domain size as the NP diameter decreases. This is perhaps similar to the effect of NP size on magnetic domains in NPs such as Fe_3O_4, where NP diameters >20 nm lead to multidomain magnetic NPs, while diameters <20 nm achieve single-domain NPs.[70,71] Since results from TA microscopy indicate that domain boundaries may be bridged by nanocrystalline and amorphous areas,[72] an increase in domain interfaces could also lead to greater disorder.

Laser power-dependence studies reveal that within the pulse energies used for the fsTA experiments, triplet exciton decay is independent of excitation density (Figure 6). However, when the fluence is >9 μJ/cm^2, the decay rate measured at 628 nm increases, requiring bimolecular kinetics to fit the data at the highest fluence (130 μJ/cm^2).[73] However, the triplet exciton decay of the data acquired at low fluences is adequately modeled using eq 1, which reflects that nongeminate triplet−triplet interactions do not significantly contribute in that regime. Largely geminate triplet exciton decay is consistent with the small domain sizes in the NPs. If the crystallites within the NPs are more poorly aligned with one another than in an annealed thin film, or if solvent penetration creates a higher barrier to triplet transport across grain boundaries, the triplet pair would be more likely to recombine instead of fully separating. Several studies have explored the nature and effect of grain boundaries on SF triplet diffusion in thin films,[64,72] although it is unclear how NPs may differ from thin films. As nucleation of the molecular precursor proceeds toward agglomerated NPs, crystallite alignment may be more random than in an annealed film or result in amorphous interstitial sites that solvent may penetrate and thereby affect triplet diffusion.

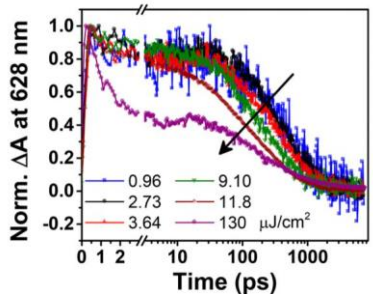

Figure 6. Normalized kinetic traces at 628 nm for 90 nm NPs, representing ground state bleach recovery as a function of excitation density.

Finally, we estimated the triplet yield across PhTDPP NP sizes at 1 ns where the spectra contain little contribution from any singlet-like features, using the extinction coefficients determined by triplet sensitization in our previous work.[29] Details are provided in the Supporting Information (Figure S8). Decay of ^{1}(TT) during its evolution to the more dissociated triplet pair results in loss of most of the generated triplets by 1 ns, with calculated triplet yields of 29 ± 4% for 63 nm NPs, 34 ± 17% for 75 nm NPs, 61 ± 35% for 90 nm NPs, and 76 ± 23% for 193 nm NPs. The triplet yield tracks closely with the triplet lifetime, τ_4.

CONCLUSIONS

PhTDPP NP solutions in water are highly stable, with no precipitation and virtually no change in their absorption spectra over the course of many months. We find that SF dynamics in PhTDPP NPs show a surface area-to-volume ratio dependence reflecting the degree of chromophore exposure to the high dielectric aqueous environment. Compared to the larger diameter NPs, SF is more rapid in the smaller NPs since a larger proportion of the molecules experiences the high dielectric environment. This leads to SF that is slightly faster than that for PhTDPP thin films. We attribute this behavior to dielectric stabilization of a high-lying virtual CT state, which engages in an increased superexchange interaction with the $^1(S_1S_0)$ and $^1(T_1T_1)$ states. Interestingly, in contrast to PhTDPP thin films, the triplet excitons in NPs do not persist for ns to μs. As the crystalline domain size increases, the triplet excitons can diffuse away from one another more easily, with the longest lifetimes observed in the largest NPs. The ability of PhTDPP NPs to generate triplet excitons in water not only provides a useful system for studying SF in polar media but also, in addition, opens up the possibility that the triplet excitons can be used to sensitize photochemical reactions in biomaterials.

ASSOCIATED CONTENT

* Supporting Information

Data on nanoparticle stability, fluorescence data, nanoparticle triplet excited state yields and properties, global analysis and pump power analysis of transient absorption data, expansion of Figure 5 (PDF)

AUTHOR INFORMATION

Corresponding Authors

*E-mail: m-wasielewski@northwestern.edu.

*E-mail: t-marks@northwestern.edu.

ORCID

Catherine M. Mauck: 0000-0002-6432-9724

Tobin J. Marks: 0000-0001-8771-0141

Michael R. Wasielewski: 0000-0003-2920-5440

Notes

The authors declare no competing financial interest.

ACKNOWLEDGMENTS

This work was supported by the Chemical Sciences, Geosciences, and Biosciences Division, Office of Basic Energy Sciences, DOE under grant no. DE-FG02-99ER14999 (M.R.W.). C.M.M. acknowledges the support of a NSF Graduate Research Fellowship under grant no. DGE-1324585. Particle size distribution measurements were performed in the Keck Biophysics facility at Northwestern University which has received support from the W.M. Keck Foundation, Northwestern University Office for Research, NIH, and the Rice Foundation. P.E.H. (nanoparticle synthesis) was supported by the Argonne-Northwestern Solar Energy Research (ANSER) Center, an Energy Frontier Research Center funded by the U.S. Department of Energy (DOE), Office of Science, Office of Basic Energy Sciences, under award number DE-SC0001059. This research used resources of the Advanced Photon Source, a U.S. Department of Energy (DOE) Office of Science User Facility operated for the DOE Office of Science by Argonne National Laboratory under Contract No. DE-AC02-06CH11357. We thank Dr. X. Zuo (Argonne National Laboratory) for his expert support on the X-ray scattering measurements.

REFERENCES

(1) Smith, M. B.; Michl, J. Singlet Fission. Chem. Rev. 2010, 110, 6891−6936.

(2) Hanna, M. C.; Nozik, A. J. Solar Conversion Efficiency of Photovoltaic and Photoelectrolysis Cells with Carrier Multiplication Absorbers. J. Appl. Phys. 2006, 100, 074510.

(3) Smith, M. B.; Michl, J. Recent Advances in Singlet Fission. Annu. Rev. Phys. Chem. 2013, 64, 361−386.

(4) Congreve, D. N.; Lee, J.; Thompson, N. J.; Hontz, E.; Yost, S. R.; Reusswig, P. D.; Bahlke, M. E.; Reineke, S.; Van Voorhis, T.; Baldo, M. A. External Quantum Efficiency above 100% in a Singlet-Exciton-Fission−Based Organic Photovoltaic Cell. Science 2013, 340, 334−337.

(5) Jadhav, P. J.; Mohanty, A.; Sussman, J.; Lee, J.; Baldo, M. A. Singlet Exciton Fission in Nanostructured Organic Solar Cells. Nano Lett. 2011, 11, 1495−1498.

(6) Ehrler, B.; Walker, B. J.; Böhm, M. L.; Wilson, M. W. B.; Vaynzof, Y.; Friend, R. H.; Greenham, N. C. In Situ Measurement of Exciton Energy in Hybrid Singlet-Fission Solar Cells. Nat. Commun. 2012, 3, 1019.

(7) Beljonne, D.; Yamagata, H.; Brédas, J. L.; Spano, F. C.; Olivier, Y. Charge-Transfer Excitations Steer the Davydov Splitting and Mediate Singlet Exciton Fission in Pentacene. Phys. Rev. Lett. 2013, 110, 226402.

(8) Ramanan, C.; Smeigh, A. L.; Anthony, J. E.; Marks, T. J.; Wasielewski, M. R. Competition between Singlet Fission and Charge Separation in Solution-Processed Blend Films of 6,13-Bis-(Triisopropylsilylethynyl)Pentacene with Sterically-Encumbered Per-ylene-3,4:9,10-Bis(dicarboximide)s. J. Am. Chem. Soc. 2012, 134, 386− 397.

(9) Sanders, S. N.; et al. Quantitative Intramolecular Singlet Fission in Bipentacenes. J. Am. Chem. Soc. 2015, 137, 8965−8972.

(10) Zimmerman, P. M.; Zhang, Z.; Musgrave, C. B. Singlet Fission in Pentacene through Multi-Exciton Quantum States. Nat. Chem. 2010, 2, 648−652.

(11) Arias, D. H.; Ryerson, J. L.; Cook, J. D.; Damrauer, N. H.; Johnson, J. C. Polymorphism Influences Singlet Fission Rates in Tetracene Thin Films. Chem. Sci. 2016, 7, 1185−1191.

(12) Burdett, J. J.; Bardeen, C. J. The Dynamics of Singlet Fission in Crystalline Tetracene and Covalent Analogs. Acc. Chem. Res. 2013, 46, 1312−1320.

(13) Burdett, J. J.; Gosztola, D.; Bardeen, C. J. The Dependence of Singlet Exciton Relaxation on Excitation Density and Temperature in Polycrystalline Tetracene Thin Films: Kinetic Evidence for a Dark Intermediate State and Implications for Singlet Fission. J. Chem. Phys. 2011, 135, 214508.

(14) Korovina, N. V.; Das, S.; Nett, Z.; Feng, X.; Joy, J.; Haiges, R.; Krylov, A. I.; Bradforth, S. E.; Thompson, M. E. Singlet Fission in a Covalently Linked Cofacial Alkynyltetracene Dimer. J. Am. Chem. Soc. 2016, 138, 617−627.

(15) Margulies, E. A.; Wu, Y.-L.; Gawel, P.; Miller, S. A.; Shoer, L. E.; Schaller, R. D.; Diederich, F.; Wasielewski, M. R. Sub-Picosecond Singlet Exciton Fission in Cyano-Substituted Diaryltetracenes. Angew. Chem., Int. Ed. 2015, 54, 8679−8683.

(16) Piland, G. B.; Bardeen, C. J. How Morphology affects Singlet Fission in Crystalline Tetracene. J. Phys. Chem. Lett. 2015, 6, 1841− 1846.

(17) Wang, C.; Angelella, M.; Kuo, C.-H.; Tauber, M. J. In Singlet Fission in Carotenoid Aggregates: Insights from Transient Absorption Spectroscopy, Proc. SPIE, Physical Chemistry of Interfaces and Nanomaterials XI, 2012; pp 845905, DOI: 10.1117/12.958612.

(18) Wang, C.; Tauber, M. J. High-Yield Singlet Fission in a Zeaxanthin Aggregate Observed by Picosecond Resonance Raman Spectroscopy. J. Am. Chem. Soc. 2010, 132, 13988−13991.
(19) Musser, A. J.; Liebel, M.; Schnedermann, C.; Wende, T.; Kehoe, T. B.; Rao, A.; Kukura, P. Evidence for Conical Intersection Dynamics Mediating Ultrafast Singlet Exciton Fission. Nat. Phys. 2015, 11, 352− 357.
(20) Ryerson, J. L.; Schrauben, J. N.; Ferguson, A. J.; Sahoo, S. C.; Naumov, P.; Havlas, Z.; Michl, J.; Nozik, A. J.; Johnson, J. C. Two Thin Film Polymorphs of the Singlet Fission Compound 1,3-Diphenylisobenzofuran. J. Phys. Chem. C 2014, 118, 12121−12132.
(21) Schrauben, J. N.; Ryerson, J. L.; Michl, J.; Johnson, J. C. Mechanism of Singlet Fission in Thin Films of 1,3-Diphenylisobenzofuran. J. Am. Chem. Soc. 2014, 136, 7363−7373.
(22) Eaton, S. W.; Miller, S. A.; Margulies, E. A.; Shoer, L. E.; Schaller, R. D.; Wasielewski, M. R. Singlet Exciton Fission in Thin Films of tert-Butyl-Substituted Terrylenes. J. Phys. Chem. A 2015, 119, 4151−4161.
(23) Eaton, S. W.; et al. Singlet Exciton Fission in Polycrystalline Thin Films of a Slip-Stacked Perylenediimide. J. Am. Chem. Soc. 2013, 135, 14701−14712.
(24) Dillon, R. J.; Piland, G. B.; Bardeen, C. J. Different Rates of Singlet Fission in Monoclinic versus Orthorhombic Crystal Forms of Diphenylhexatriene. J. Am. Chem. Soc. 2013, 135, 17278−17281.
(25) Monahan, N.; Zhu, X. Y. Charge Transfer−Mediated Singlet Fission. Annu. Rev. Phys. Chem. 2015, 66, 601−618.
(26) Varnavski, O.; Abeyasinghe, N.; Arago,́J.; Serrano-Perez,́ J. J.; Ortí, E.; Lopeź Navarrete, J. T.; Takimiya, K.; Casanova, D.; Casado, J.; Goodson, T. High Yield Ultrafast Intramolecular Singlet Exciton Fission in a Quinoidal Bithiophene. J. Phys. Chem. Lett. 2015, 6, 1375− 1384.
(27) Busby, E.; Xia, J.; Wu, Q.; Low, J. Z.; Song, R.; Miller, J. R.; Zhu, X. Y.; Campos, L. M.; Sfeir, M. Y. A Design Strategy for Intramolecular Singlet Fission Mediated by Charge-Transfer States in Donor-Acceptor Organic Materials. Nat. Mater. 2015, 14, 426−433.
(28) Casanova, D.; Krylov, A. I. Quantifying Local Exciton, Charge Resonance, and Multiexciton Character in Correlated Wave Functions of Multichromophoric Systems. J. Chem. Phys. 2016, 144, 014102.
(29) Hartnett, P. E.; Margulies, E. A.; Mauck, C. M.; Miller, S. A.; Wu, Y.; Wu, Y.-L.; Marks, T. J.; Wasielewski, M. R. Effects of Crystal Morphology on Singlet Exciton Fission in Diketopyrrolopyrrole Thin Films. J. Phys. Chem. B 2016, 120, 1357−1366.
(30) Chandran, D.; Lee, K.-S. Diketopyrrolopyrrole: A Versatile Building Block for Organic Photovoltaic Materials. Macromol. Res. 2013, 21, 272−283.
(31) Li, Y.; Sonar, P.; Murphy, L.; Hong, W. High Mobility Diketopyrrolopyrrole (DPP)-Based Organic Semiconductor Materials for Organic Thin Film Transistors and Photovoltaics. Energy Environ. Sci. 2013, 6, 1684−1710.
(32) Naik, M. A.; Patil, S. Diketopyrrolopyrrole-Based Conjugated Polymers and Small Molecules for Organic Ambipolar Transistors and Solar Cells. J. Polym. Sci., Part A: Polym. Chem. 2013, 51, 4241−4260.
(33) Grzybowski, M.; Gryko, D. T. Diketopyrrolopyrroles: Synthesis, Reactivity, and Optical Properties. Adv. Opt. Mater. 2015, 3, 280−320.
(34) Qu, S.; Tian, H. Diketopyrrolopyrrole-Based Materials for Organic Photovoltaics. Chem. Commun. 2012, 48, 3039−3051.
(35) Brown, K. E.; Salamant, W. A.; Shoer, L. E.; Young, R. M.; Wasielewski, M. R. Direct Observation of Ultrafast Excimer Formation in Covalent Perylenediimide Dimers using near-Infrared Transient Absorption Spectroscopy. J. Phys. Chem. Lett. 2014, 5, 2588−2593.
(36) Katoh, R.; Katoh, E.; Nakashima, N.; Yuuki, M.; Kotani, M. Near-IR Absorption Spectrum of Aromatic Excimers. J. Phys. Chem. A 1997, 101, 7725−7728.
(37) Katoh, R.; Sinha, S.; Murata, S.; Tachiya, M. Origin of the Stabilization Energy of Perylene Excimer as Studied by Fluorescence and near-IR Transient Absorption Spectroscopy. J. Photochem. Photobiol., A 2001, 145, 23−34.
(38) Kirkus, M.; Janssen, R. A. J.; Meskers, S. C. J. Intramolecular Excimer Formation between 3,6-Di(thiophen-2-yl)pyrrolo[3,4-c]-Pyrrole-1,4(2H,5H)-Dione Chromophoric Groups Linked by a Flexible Alkyl Spacer. J. Phys. Chem. A 2013, 117, 4828−4837.
(39) Miller, C. E.; Wasielewski, M. R.; Schatz, G. C. Modeling Singlet Fission in Rylene and Diketopyrrolopyrrole Derivatives: The Role of the Charge Transfer State in Superexchange and Excimer Formation. J. Phys. Chem. C 2017, 121, 10345−10350.
(40) Mastron, J. N.; Roberts, S. T.; McAnally, R. E.; Thompson, M. E.; Bradforth, S. E. Aqueous Colloidal Acene Nanoparticles: A New Platform for Studying Singlet Fission. J. Phys. Chem. B 2013, 117, 15519−15526.
(41) Pensack, R. D.; et al. Exciton Delocalization Drives Rapid Singlet Fission in Nanoparticles of Acene Derivatives. J. Am. Chem. Soc. 2015, 137, 6790−6803.
(42) Lim, S.-H.; Bjorklund, T. G.; Spano, F. C.; Bardeen, C. J. Exciton Delocalization and Superradiance in Tetracene Thin Films and Nanoaggregates. Phys. Rev. Lett. 2004, 92, 107402.
(43) Tayebjee, M. J. Y.; Schwarz, K. N.; MacQueen, R. W.; Dvorak̃, M.; Lam, A. W. C.; Ghiggino, K. P.; McCamey, D. R.; Schmidt, T. W.; Conibeer, G. J. Morphological Evolution and Singlet Fission in Aqueous Suspensions of TIPS-Pentacene Nanoparticles. J. Phys. Chem. C 2016, 120, 157−165.
(44) Abrahamse, H.; Hamblin, M. R. New Photosensitizers for Photodynamic Therapy. Biochem. J. 2016, 473, 347−364.
(45) Liu, Y.; Buru, C. T.; Howarth, A. J.; Mahle, J. J.; Buchanan, J. H.; DeCoste, J. B.; Hupp, J. T.; Farha, O. K. Efficient and Selective Oxidation of Sulfur Mustard Using Singlet Oxygen Generated by a Pyrene-Based Metal-Organic Framework. J. Mater. Chem. A 2016, 4, 13809−13813.
(46) Nakanishi, H.; Oikawa, H. Reprecipitation Method for Organic Nanocrystals. In Single Organic Nanoparticles; Masuhara, H., Nakanishi, H., Sasaki, K., Eds.; Springer Berlin Heidelberg: Berlin, Heidelberg, 2003; pp 17−31, DOI: 10.1007/978-3-642-55545-9_2.
(47) Filipe, V.; Hawe, A.; Jiskoot, W. Critical Evaluation of Nanoparticle Tracking Analysis (NTA) by Nanosight for the Measurement of Nanoparticles and Protein Aggregates. Pharm. Res. 2010, 27, 796−810.
(48) Bu̇rckstu̇mmer, H.; Weissenstein, A.; Bialas, D.; Wu̇rthner, F. Synthesis and Characterization of Optical and Redox Properties of Bithiophene-Functionalized Diketopyrrolopyrrole Chromophores. J. Org. Chem. 2011, 76, 2426−2432.
(49) Naik, M. A.; Venkatramaiah, N.; Kanimozhi, C.; Patil, S. Influence of Side-Chain on Structural Order and Photophysical Properties in Thiophene Based Diketopyrrolopyrroles: A Systematic Study. J. Phys. Chem. C 2012, 116, 26128−26137.
(50) Dhar, J.; Karothu, D. P.; Patil, S. Herringbone to Cofacial Solid State Packing Via H-Bonding in Diketopyrrolopyrrole (DPP) Based Molecular Crystals: Influence on Charge Transport. Chem. Commun. 2015, 51, 97−100.
(51) Smilgies, D.-M. Scherrer Grain-Size Analysis Adapted to Grazing-Incidence Scattering with Area Detectors. J. Appl. Crystallogr. 2009, 42, 1030−1034.
(52) Young, R. M.; et al. Charge Transport across DNA-Based Three-Way Junctions. J. Am. Chem. Soc. 2015, 137, 5113−5122.
(53) Mauck, C. M.; Hartnett, P. E.; Margulies, E. A.; Ma, L.; Miller, C. E.; Schatz, G. C.; Marks, T. J.; Wasielewski, M. R. Singlet Fission via an Excimer-Like Intermediate in 3,6-Bis(Thiophen-2-yl)-Diketopyrrolopyrrole Derivatives. J. Am. Chem. Soc. 2016, 138, 11749−11761.
(54) Felker, P. M.; Zewail, A. H. Dynamics of Intramolecular Vibrational-Energy Redistribution (IVR). II. Excess Energy Depend-ence. J. Chem. Phys. 1985, 82, 2975−2993.
(55) Rafiq, S.; Scholes, G. D. Slow Intramolecular Vibrational Relaxation Leads to Long-Lived Excited-State Wavepackets. J. Phys. Chem. A 2016, 120, 6792−6799.
(56) Yamaguchi, S.; Hamaguchi, H.-o. Ultrafast Vibrational Relaxation in Photogenerated S_1 α-Terthiophene in Solution by Femtosecond Time-Resolved Absorption/Emission and Picosecond Time-Resolved Raman Spectroscopy. Chem. Phys. Lett. 1994, 227, 255−260.

(57) Kirkus, M.; Wang, L.; Mothy, S.; Beljonne, D.; Cornil, J.; Janssen, R. A. J.; Meskers, S. C. J. Optical Properties of Oligothiophene Substituted Diketopyrrolopyrrole Derivatives in the Solid Phase: Joint J- and H-Type Aggregation. J. Phys. Chem. A 2012, 116, 7927−7936.

(58) Basel, B. S.; et al. Unified Model for Singlet Fission within a Non-Conjugated Covalent Pentacene Dimer. Nat. Commun. 2017, 8, 15171.

(59) Weiss, L. R.; Bayliss, S. L.; Kraffert, F.; Thorley, K. J.; Anthony, J. E.; Bittl, R.; Friend, R. H.; Rao, A.; Greenham, N. C.; Behrends, J. Strongly Exchange-Coupled Triplet Pairs in an Organic Semi-conductor. Nat. Phys. 2017, 13, 176−181.

(60) Tayebjee, M. J. Y.; Sanders, S. N.; Kumarasamy, E.; Campos, L. M.; Sfeir, M. Y.; McCamey, D. R. Quintet Multiexciton Dynamics in Singlet Fission. Nat. Phys. 2017, 13, 182−188.

(61) Roberts, S. T.; McAnally, R. E.; Mastron, J. N.; Webber, D. H.; Whited, M. T.; Brutchey, R. L.; Thompson, M. E.; Bradforth, S. E. Efficient Singlet Fission Discovered in a Disordered Acene Film. J. Am. Chem. Soc. 2012, 134, 6388−6400.

(62) Bayliss, S. L.; Chepelianskii, A. D.; Sepe, A.; Walker, B. J.; Ehrler, B.; Bruzek, M. J.; Anthony, J. E.; Greenham, N. C. Geminate and Nongeminate Recombination of Triplet Excitons Formed by Singlet Fission. Phys. Rev. Lett. 2014, 112, 238701.

(63) Zhu, T.; Wan, Y.; Guo, Z.; Johnson, J.; Huang, L. Two Birds with One Stone: Tailoring Singlet Fission for Both Triplet Yield and Exciton Diffusion Length. Adv. Mater. 2016, 28, 7539−7547.

(64) Grieco, C.; Doucette, G. S.; Pensack, R. D.; Payne, M. M.; Rimshaw, A.; Scholes, G. D.; Anthony, J. E.; Asbury, J. B. Dynamic Exchange During Triplet Transport in Nanocrystalline Tips-Pentacene Films. J. Am. Chem. Soc. 2016, 138, 16069−16080.

(65) Lukman, S.; et al. Tuneable Singlet Exciton Fission and Triplet− Triplet Annihilation in an Orthogonal Pentacene Dimer. Adv. Funct. Mater. 2015, 25, 5452−5461.

(66) Scholes, G. D. Correlated Pair States Formed by Singlet Fission and Exciton−Exciton Annihilation. J. Phys. Chem. A 2015, 119, 12699−12705.

(67) Poletayev, A. D.; Clark, J.; Wilson, M. W. B.; Rao, A.; Makino, Y.; Hotta, S.; Friend, R. H. Triplet Dynamics in Pentacene Crystals: Applications to Fission-Sensitized Photovoltaics. Adv. Mater. 2014, 26, 919−924.

(68) Wan, Y.; Guo, Z.; Zhu, T.; Yan, S.; Johnson, J.; Huang, L. Cooperative Singlet and Triplet Exciton Transport in Tetracene Crystals Visualized by Ultrafast Microscopy. Nat. Chem. 2015, 7, 785− 792.

(69) Najafov, H.; Lee, B.; Zhou, Q.; Feldman, L. C.; Podzorov, V. Observation of Long-Range Exciton Diffusion in Highly Ordered Organic Semiconductors. Nat. Mater. 2010, 9, 938−943.

(70) Kolhatkar, A. G.; Jamison, A. C.; Litvinov, D.; Willson, R. C.; Lee, T. R. Tuning the Magnetic Properties of Nanoparticles. Int. J. Mol. Sci. 2013, 14, 15977−16009.

(71) Lu, A.-H.; Salabas, E. L.; Schüth, F. Magnetic Nanoparticles: Synthesis, Protection, Functionalization, and Application. Angew. Chem., Int. Ed. 2007, 46, 1222−1244.

(72) Wong, C. Y.; Cotts, B. L.; Wu, H.; Ginsberg, N. S. Exciton Dynamics Reveal Aggregates with Intermolecular Order at Hidden Interfaces in Solution-Cast Organic Semiconducting Films. Nat. Commun. 2015, 6, 5946.

(73) Howard, I. A.; Laquai, F.; Keivanidis, P. E.; Friend, R. H.; Greenham, N. C. Perylene Tetracarboxydiimide as an Electron Acceptor in Organic Solar Cells: A Study of Charge Generation and Recombination. J. Phys. Chem. C 2009, 113, 21225−21232.